Mid-IR band strength, density, refrative index, and thermal evolution study for solid CH_2DOH pure and in astrophysical relevant mixtures

C. Scirè[a,*], R. G. Urso[a,b], D. Fulvio[c], G. A. Baratta[a], M. E. Palumbo[a]

[a] *INAF - Osservatorio Astrofisico di Catania, via Santa Sofia 78, I-95123 Catania, Italy*
[b] *Institut d'Astrophysique Spatiale, CNRS / Université Paris-Sud, Université Paris-Saclay, btiment 121, Université Paris-Sud, 91405 Orsay Cedex, France*
[c] *Departamento de Fsica, Pontifcia Universidade Catlica do Rio de Janeiro, Rua Marqus de So Vicente 225, 22451-900, Rio de Janeiro, RJ, Brazil*

Abstract

We present a novel experimental study on solid CH_2DOH pure and in astrophysical relevant mixtures. Solid samples were accreted under ultra high vacuum conditions at 17 K and were analyzed by mid-infrared transmission spectroscopy. Refractive index, density, and mid-IR band strength values were measured for pure solid CH_2DOH. The refractive index was also measured for CH_2DOH:H_2O, CH_2DOH:CO, and CH_2DOH:CH_3OH mixtures. For all samples the thermal evolution of the main band profile was studied. We used the interference laser technique (He-Ne laser, λ= 543.5 nm) to measure the samples thickness and a numerical method to measure the refractive index starting from the amplitude of the interference curve. We obtained the ice density through the Lorentz-Lorenz relation. To calculate the band strength values we used the linear fit of the integrated band intensities with respect to the column densities. Samples deposited at 17 K were warmed up to their sublimation temperature. Spectra were taken at selected temperatures to study their thermal evolution. The results are discussed in view of their relevance for the interpretation of astronomical IR spectra.

Keywords: IR spectroscopy - astrochemistry - solid state - ISM:molecules - deuterated methanol - IR band strength

*Corresponding author at: INAF - Catania Astrophysical Observatory, via Santa Sofia 78, I-95123 Catania, Italy

Email address: carlotta.scire@inaf.it (C. Scirè)

1. Introduction

The star formation process takes place in dense molecular clouds. Astronomical observations toward these objects at radio wavelengths clearly show the presence of emission lines assigned to gas phase molecules. To date about two hundreds molecular species have been identified in interstellar and circumstellar regions[1]. In addition infrared observations clearly show the presence of absorption features superimposed to the continuum radiation emitted by young stellar objects still embedded in their parental cloud. It is largely accepted that these features are due to solid phase molecules which, because of the low temperature (as low as 10 K), freeze out and form a coating (often referred to as ice mantle) on dust grains also present in molecular clouds. About 10 molecular species have been identified in ice mantles. Among them the most abundant are H_2O, CO, CO_2, and CH_3OH. However it is largely believed that other species are also present in the solid phase, not yet detected due to the limits of presently available astronomical instrumentation (e.g. Boogert et al., 2015).

The identification and assignment of the observed absorption bands is based on the comparison between astronomical and laboratory spectra of relevant species and their mixtures in the solid phase. Furthermore, when infrared transmittance astronomical spectra are converted to optical depth scale the column density (molecules cm^{-2}) of the species responsible of a given absorption band can be obtained if the band strength value (in units of cm $molecule^{-1}$) is known. Since the first detections of solid phase molecules in dense molecular clouds (e.g. Gillett et al., 1973; Tielens et al., 1991; Allamandola et al., 1992) several experimental works have focused on the measurement of band strength values of astronomical relevant molecules (e.g. Hudgins et al., 1993; Schutte et al., 1993; Gerakines et al., 1995; Mulas et al., 1998; Palumbo et al., 1999; Kerkhof et al., 1999; berg et al., 2015; Fulvio et al., 2009; Modica & Palumbo, 2010; Luna et al., 2018).

Isotopologues have also been detected in star-forming regions. In particular ^{13}CO and $^{13}CO_2$ have been identified in icy grain mantles (e.g. Boogert et al., 2000, 2002; Gibb et al., 2004). In addition, other isotopologues, such as $C^{18}O$ and $C^{17}O$, HD, HDO, D_2O, HDCO, CH_2DOH, and CH_3OD, have

[1] http://www.astrochymist.org/astrochymist_ism.html

been detected in the gas phase (e.g. Ceccarelli et al., 2002; Fontani et al., 2014, 2015; Bianchi et al., 2017).

According to current models, in dense molecular clouds, deuterated species (such as HDO and CH_2DOH) form in the solid phase and are released to the gas phase with the desorption of ice mantles. As a matter of fact the absorption feature due to solid HDO has been extensively searched for and its identification is still highly debated (Teixeira et al., 1999; Dartois et al., 2003; Parise et al., 2003; Aikawa et al., 2012; Urso et al., 2018). Gas-phase isotopologues have been also identified in the Solar System (Hartogh et al., 2011; Altwegg et al., 2015; Furi and Marthy, 2015), while they have never been detected in the solid-phase on the surface of solar system bodies. It has been suggested that the study of astrophysical relevant deuterated species could be a key aspect in order to better understand the Solar System formation (e.g. Ceccarelli et al., 2014) and the link between the composition of interstellar material and primitive bodies (e.g. Greenberg , 1982; Caselli and Ceccarelli, 2012; berg et al., 2015; Altwegg et al., 2017; Drozdovskaya et al., 2018).

To the best of our knowledge the detection in space of solid deuterated methanol has never been reported. However in the near future the James Webb Space Telescope will be operative. Thanks to its high sensitivity it will be used to search for less abundant species and in particular for deuterated species. With this is mind we have performed a novel experimental investigation to measure the band strength values of the main infrared bands of solid methanol-1-d (CH_2DOH) and to study the profile of the bands of pure solid CH_2DOH and its mixtures with H_2O, CO, and CH_3OH at low temperature and during warm-up to its sublimation temperature. In particular, we focus on the C-D stretching mode bands in the 2300-2100 cm^{-1} spectral region, because these features are not present in the spectrum of CH_3OH and will be used to search for CH_2DOH in astronomical spectra.

2. Experimental methods and setup

Six different sets of experiments were performed in the Laboratory for Experimental Astrophysics at INAF-Osservatorio Astrofisico di Catania (Italy), in order to obtain information on the thermal evolution of pure CH_3OH, CD_3OD and CH_2DOH and mixtures containing CH_2DOH:CO=1:4, CH_2DOH: H_2O=1:5 and CH_2DOH:CH_3OH=1:2 deposited at 17 K. Refractive index and, in the case of pure species, also the density of the deposited frozen films

have been evaluated. To perform the deposition, we used vapors of CD_3OD from liquid ampoule by Aldrich Chemical (99.95 atom % D), of CH_3OH from liquid ampoule by Merck and of CH_2DOH (Methanol-1-d) from liquid ampoule by Sigma Aldrich with nominal isotopic purity of 98 atom % D. The CH_2DOH:CO=1:4 mixture was prepared by using a CO gas cylinder (Aldrich Chemical, 99%) end for the CH_2DOH:H_2O=1:5 mixture we used vapors produced from liquid H_2O (Chromasolv Plus by Sigma Aldrich). The experimental set-up is composed by an ultra high vacuum (UHV) stainless steel chamber (pressure $P < 10^{-9}$ mbar) interfaced with a FTIR spectrophotometer through IR-transparent windows (KBr). The gas mixture is prepared in a separate mixing chamber, previously evacuated at a pressure lower than 10^{-6} mbar, and is admitted through a flow regulating valve in the UHV main chamber. A gas inlet allows to introduce the gas mixture into the chamber where it freezes on a substrate (in this work KBr) placed in thermal contact with the final tail of a closed-cycle helium cryostat which reaches the temperature of 17 K. The temperature of the substrate can be therefore varied in the range 17-300 K by using a resistor coupled with a diode temperature sensor based controller. The samples were deposited at 17 K and subjected to several steps of warm up until their complete sublimation. All the steps were analyzed acquiring infrared transmission spectra (8000-400 cm^{-1}) by a Fourier transform infrared (FTIR) spectrophotometer (Bruker Vertex 70) with a resolution of 1 cm^{-1}. **Each datapoint (sampling) is given every 0.25 cm^{-1} that corresponds to 1/4 of the resolution.** Thanks to a rotatable polarizer placed along the path of the IR beam, spectra were taken both in P and S polarizations, where the electric vector is parallel (P) or perpendicular (S) to the plane of incidence. The substrate surface is inclined by an angle of 45° with respect to the infrared beam. A transparent window in the UHV chamber allows the thickness measurement during the deposition by using an external He-Ne laser (λ = 543.5 nm) reflected at near normal incidence (2.35° vertical tilt) by the ice film deposited on the substrate. The gas inlet, **placed at the bottom of the vacuum chamber**, is not directed toward the substrate in order to obtain a background deposition and hence a uniform thickness of the ice film. **For each sample the deposition rate was kept constant. It values about 0.7 μm/h in the case of the CH_2DOH:H_2O mixture and ranges from 2.5 to 3.4 μm/h in the case of the other samples.** The ice deposition on the backside of the substrate is avoided by using a copper tube which is 2 cm long and has a diameter of 0.45 cm. The tube is attached to the sample holder (on

the opposite side of the substrate) along the IR beam direction. **As a consequence, only a negligible fraction of the molecules that deposit on the front surface of the substrate can stick on the back surface of it. That is, only the molecules entering the tube and passing through it without sticking on its inner walls.** A cold copper thermal radiation shield is attached to the first stage of the cryostat along the cold finger vertical axis. In Fig. 1 a schematic drawing of the UHV chamber is reported, the cold shield is omitted for better clarity.

2.1. Thickness measurements

As described in Fulvio et al. (2009), Modica & Palumbo (2010), and Urso et al. (2016) during the deposition it is possible to measure the ice film thickness by using the laser interference technique. A laser beam directed towards a two layers system composed by a thin ice film deposited on a substrate (Fig. 2), produces reflections at the interfaces vacuum-ice and ice-substrate. The reflected beams give the characteristic interference pattern that provides ice thickness information. In our experimental setup, a He-Ne laser (λ = 543.5 nm) is reflected on the sample at near normal incidence (θ_i=2.35°). The reflected beam is detected by an external silicon-diode detector and its intensity is recorded by a computer routine. The substrate used in this work is a KBr disk. In general the amplitude of the interference curve depends on the refractive index of the film, so we can derive this quantity by using a FORTRAN routine (Baratta and Palumbo, 1998) and then measure the thickness by comparing the experimental interference curve (an example for CH_2DOH is shown in Fig. 3 (a)) with the theoretical curve provided by the routine (Fig. 3 (b)). The comparison procedure is described in Urso et al. (2016). The FORTRAN routine can be run on line through a free web user interface available at the link: http://www.oact.inaf.it/thickness/. By entering in the web user interface some information such as the ratio between the minimum and the maximum of the experimental interference curve, the laser wavelength, the angle of incidence, the substrate and the polarization (P or S) of the laser beam, the routine will provide the theoretical interference curve finding the refractive index of the film by varying the n_f value (where n_f is the refractive index of the film) until the theoretical interference curve has the same amplitude of the experimental one.

In Fig. 3(a) vertical lines indicate the time when the deposition was stopped and infrared spectra were taken. The acquisition of each spectrum (which is the addition of 120 spectra) takes about

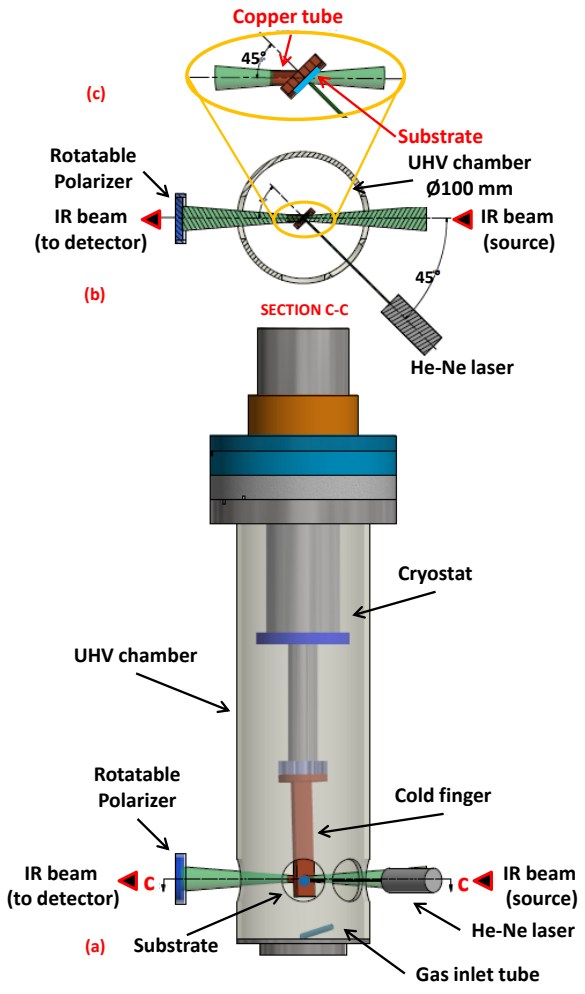

Figure 1: (a) Three-dimensional drawing of the UHV chamber system. (b) Top view section of the chamber. **(c) Detail of the copper tube used to avoid gas deposition on the backside of the substrate (not to scale).**

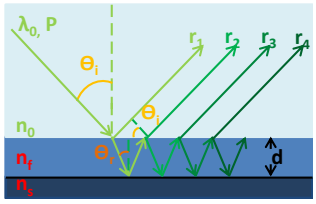

Figure 2: Multiple reflections are produced by a laser beam (with wavelength λ_0 and polarization P) directed towards a two layer system where n_f is the refractive index of the film, n_s is the refractive index of the substrate, θ_i is the incidence angle and θ_r is the angle of refraction.

6 minutes. In principle we could reduce the number of total added spectra in order to reduce the acquisition time to allow the laser intensity measurement and IR spectroscopy at the same time without stopping the deposition. However this would decrease the signal to noise ratio of the final spectra and each spectrum would correspond to an average value of the thickness range. Both effects would worsen the final results.

From the Snells law we can derive the effective thickness seen by the IR beam coming at oblique incidence (45°) into the ice-film (see Fig. 4). In particular if we indicate with d_{eff} the effective thickness we find:

$$d_{eff} = \frac{d}{cos\theta_r} = \frac{d}{\sqrt{1 - sin^2\theta_i n_0^2/n_f^2}} \quad (1)$$

where n_0 is the refractive index of the vacuum, n_f is the refractive index of the ice-film obtained from the amplitude of the interference curve, θ_i is the incidence angle of the IR beam (θ_i=45°) and θ_r is the refractive angle. In the previous relation we neglect any variation of the refractive index with wavelength (dispersion) from the laser to the mid infrared wavelengths.

3. Results

3.1. Refractive index and density

Once the refractive index is derived, as described above, it is possible to estimate the film density using the Lorentz-Lorenz relation (eq. 2) where L is the Lorentz-Lorenz coefficient and ρ is the density. In particular for a given material, the Lorentz-Lorenz coefficient is nearly constant independently of the material phase and temperature (Wood and Roux, 1982).

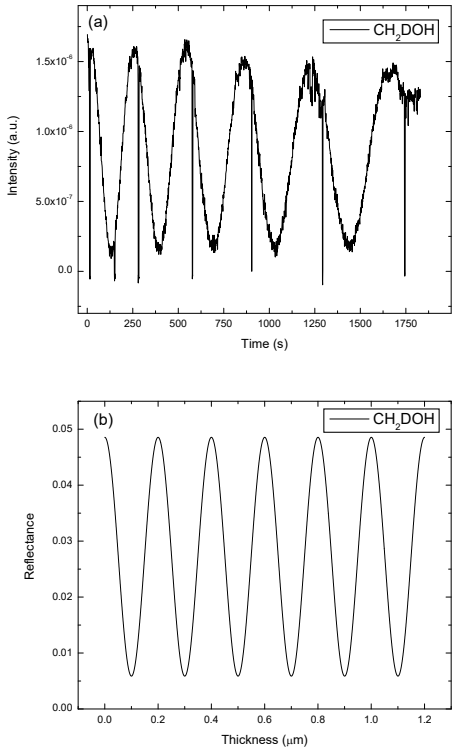

Figure 3: (a) Experimental interference curve for the CH_2DOH pure ice. Sharp changes **(vertical lines)** in the laser intensity indicate the time when the deposition was stopped and an IR spectrum was taken. After that deposition was restarted. (b) Theoretical interference curve for the CH_2DOH pure ice.

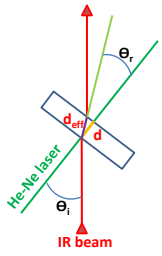

Figure 4: Schematic view of the geometry used for the measure of the effective sample thickness.

Table 1: Reference values of refractive index **(λ= 589.3 nm)** and density for pure species.

Species	Phase	T (°C)	Refractive index	Density (g/cm^3)	References
CH_3OH	liquid	25	1.33	0.79	ddbst.com
CD_3OD	liquid	20	1.33	0.89	sigmaaldrich.com
CH_2DOH	liquid	20	1.33	0.82	sigmaaldrich.com

$$L\rho = \frac{n_f^2 - 1}{n_f^2 + 2} \tag{2}$$

By using the reference values of refractive index and density reported in Table 1, and the refractive index measured for the ice films deposited at 17 K, we have computed the density of the pure solid species through the Lorentz-Lorenz relation. The resulting refractive index and density of the pure species in the solid phase CH_3OH, CD_3OD and CH_2DOH are reported in Table 2. **It is interesting to note that the density increases proportionally with the molecular weight of the isotopologue. This suggests that the arrangement of the molecules in the three different samples is the same and the density only depends on the mass of the species.**

Recently the density and the refractive index of pure CH_3OH have been measured by Luna et al. (2018). For the measurement at 20 K they found 0.64 g/cm^3 and 1.26 for the density and refractive index values, respectively. These values are quite different from those reported in Table 2. As discussed by Loeffler et al. (2016) and Baratta and Palumbo (2017) the density and in turn the refractive index of solid phase molecules strongly depends on the experimental conditions such as substrate temperature, deposition rate, and growth angle. As a consequence, the comparison between experimental values obtained in different laboratories is not straightforward and this may explain the discrepancies here outlined.

Since Eq. 2 cannot be directly applied for ice mixtures, in these cases only the refractive index values were determined (by the interference curve method) and they are reported in Table 3.

Our method of measurement of refractive index is affected by an error lower than 1%.

Table 2: Refractive index **(λ= 543.5 nm)** and density values measured in this work for pure solid species.

Species	Phase	T (K)	Refractive index	Density (g/cm^3)
CH_3OH	solid	17	1.36	0.85
CD_3OD	solid	17	1.35	0.96
CH_2DOH	solid	17	1.35	0.87

Table 3: Refractive index values **(λ= 543.5 nm)** for mixtures studied in this work.

Species	Ratio	Phase	T (K)	Refractive index
CH_2DOH:CO	1:4	solid	17	1.31
CH_2DOH:H_2O	1:5	solid	17	1.32
CH_2DOH:CH_3OH	1:2	solid	17	1.36

3.2. Band strength values

If we indicate with M the molar mass (g mole^{-1}) of a given pure species and with N_A the Avogadro constant, the column density N (molecules cm^{-2}) is given by the relation:

$$N = \frac{\rho d_{eff} N_A}{M} \tag{3}$$

where d_{eff} is the effective thickness (cm) and ρ is the density (g cm^{-3}) of the ice film. All the transmittance spectra reported in this article are given in optical depth scale. The optical depth (τ) was calculated by using the Beer-Lambert law: I=$I_0 e^{-\tau}$ where I_0 is the normalization continuum. The band strength A(cm molecule^{-1}) of a given band is obtained by the relation (e.g. Modica & Palumbo, 2010):

$$A = \frac{\int \tau(\nu) d\nu}{N} \tag{4}$$

where $\int \tau(\nu) d\nu$ is the band area (cm^{-1}). In order to obtain the band strength values from a linear best fit procedure, during the deposition, spectra were acquired at different film thickness. As an example, the IR spectra acquired during the deposition of CH_2DOH are reported in Fig. 5.

For a given band, we have plotted the band area versus the column density computed by using eq. 3 at each intermediate deposition step and related

d_{eff}. The band strength (A) of each considered feature was therefore determined as the slope of the linear best fit to the data.

3.2.1. CH_2DOH

In Fig. 5 all the CH_2DOH bands have been assigned. Table 4 reports their positions and reference values obtained by matrix isolation spectroscopy studies (Serrallach et al., 1974; Shimoaka and Katsumoto, 2010). As discussed by Shimoaka and Katsumoto (2010), three bands are evident in the spectral region (2150-2290 cm^{-1}) for CH_2DOH. These bands are not observed in CH_3OH ice (Fig. 6) and are due to CD stretching modes. In the present work they are observed at 2244, 2179 and 2144 cm^{-1}. **Following Shimoaka and Katsumoto (2010) the 2144 cm^{-1} is assigned to $\nu_{CD}(C_1)$ mode due to the gauche conformer in which the dihedral angle D-C-O-H is close to $\pm 60°$, the 2244 cm^{-1} band is assigned to $\nu_{CD}(C_s)$ mode which arises from the trans conformer with D-C-O-H equal to 180°, the 2179 cm^{-1} band results from the $\nu_{CD}(C_1)$ band of a methanol complex.** The weak band peaked at about 2240 cm^{-1} present in the spectrum of pure CH_3OH is assigned to the overtone of the ν_{11} and ν_7 modes (Bennett et al., 2007).

For these bands we have estimated the single peak A-value. To calculate the area of each component we performed a 3-component fit. We made the same estimation for the features observed at 1327 and 1265 cm^{-1} (assigned to CH_2 wagging and twisting modes respectively).

For some features, we observed a significantly different profile in P and S polarization, in this case we used the S polarized spectra to compute the band strength values. As an example the profiles of the CO stretching mode in CH_2DOH in the spectra taken in P and S polarization are shown in Fig. 7. Indeed when the profile of a given feature is different in P and S polarization, only the S profile is equivalent to the spectrum acquired at normal incidence for which the band strength values are usually given in literature (see Baratta and Palumbo, 1998; Palumbo et al., 2006). When the P and S profiles were nearly the same for a given feature, we used the P polarized spectra to compute the band strength values, this because the P polarized spectra are less affected by the interference pattern seen in the continuum with respect to the S polarized spectra (see Fig. 8, 9, 10, and 11). The band strength values measured for CH_2DOH and the corresponding peak position are reported in Table 5.

Following the same procedure we have also measured the band strength

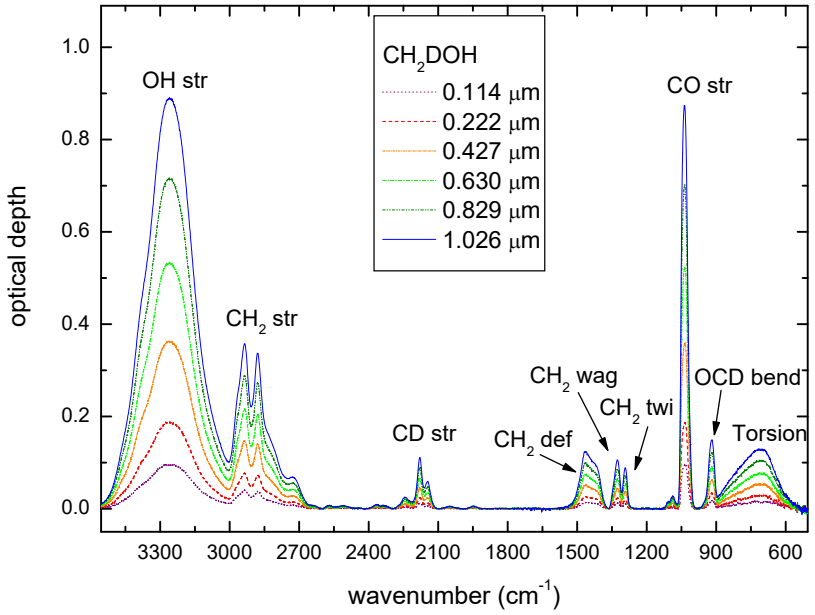

Figure 5: IR spectra of CH_2DOH ice acquired at various thicknesses in P polarization.

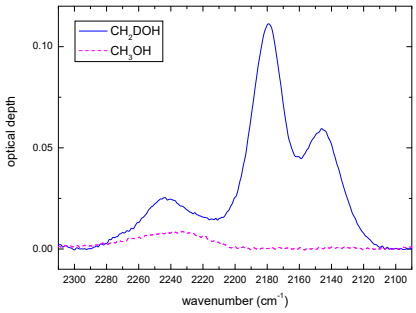

Figure 6: 2300-2100 cm^{-1} spectral region region for CH_3OH and CH_2DOH. The samples are about 1 μm thick.

Table 4: Bands assignment for pure CH_2DOH at 17 K and comparison with the literature data available for CH_2DOH in matrix isolation spectroscopy studies.

Band position (cm^{-1})[a]	Mode	Literature values (cm^{-1})[b]	Literature values (cm^{-1})[c]
3272	OH stretching	3668	
2936	CH_2 stretching	2996, 2948	
2881	CH_2 stretching	2890	
2244	CD stretching	2192, 2165	2235
2179	CD stretching	2192, 2165	2193
2144	CD stretching	2192, 2165	2165
1465	CH_2 deformation	1468, 1462	
1327	CH_2 wagging	1378, 1368	
1265	CH_2 twisting	1345, 1301	
1035	CO stretching	1052, 1025	
920	OCD bending	920, 892	
712	torsion		

[a] This work (17 K),
[b] Ar-matrix (15 K), Serrallach et al. (1974),
[c] Ar-matrix (12 K), Shimoaka and Katsumoto (2010).

Table 5: Band strength values of CH_2DOH at 17 K.

Peak position (cm^{-1})	A (cm $molecule^{-1}$)
2244	1.15 x 10^{-18}
2179	2.09 x 10^{-18}
2144	1.22 x 10^{-18}
1327	1.74 x 10^{-18}
1265	9.04 x 10^{-19}
1035	1.49 x 10^{-17}
920	1.99 x 10^{-18}

Table 6: CO stretching mode band position and A value for CH_3OH, CH_2DOH and CD_3OD.

Species	Peak position (cm^{-1})		A (cm molecule^{-1})
	This work	Literature	
CH_3OH	1031	**1027**[a]	**1.61 x 10^{-17}**[a]
CH_2DOH	1035	1052, 1025[b]	1.49 x 10^{-17}[d]
CD_3OD	975	989[c]	8.60 x 10^{-18}[d]

[a] **Pure ice (20 K), Luna et al. (2018),**
[b] Ar-matrix (15 K), Serrallach et al. (1974),
[c] Ar-matrix (15 K), Falk and Whalley (1961),
[d] Pure ice (17 K), this work.

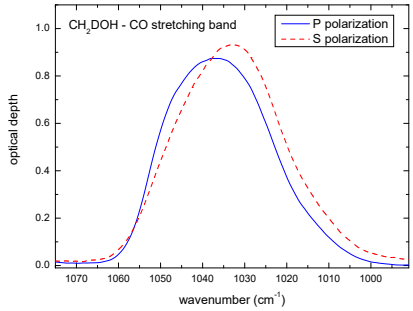

Figure 7: Comparison between P and S polarization CO stretching mode band for CH_2DOH (1035 cm^{-1}) in a sample 1.026 μm thick.

value for the CO stretching mode in CD_3OD. The best fit result is reported in Fig. 10. In Table 6 are reported the peak position and the band strength values of the CO stretching mode band for CH_3OH, CH_2DOH and CD_3OD according to our results and to literature values. **Luna et al. (2018) have measured the band strength values of CH3OH deposited on a Si substrate. In the present work a KBr substrate is used. As shown by Modica & Palumbo (2010) and Fulvio et al. (2009) the band strength values could strongly depend on the substrate. Therefore a comparison between the experimental values obtained in different laboratories using different substrates is not straightforward.**

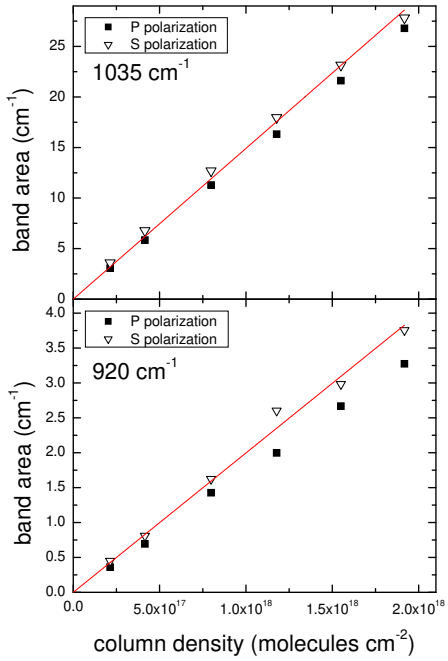

Figure 8: Measures of the CH_2DOH band areas (920 and 1035 cm^{-1}) in P and S polarization versus the column densities. The linear best fit is performed only on the S polarization data.

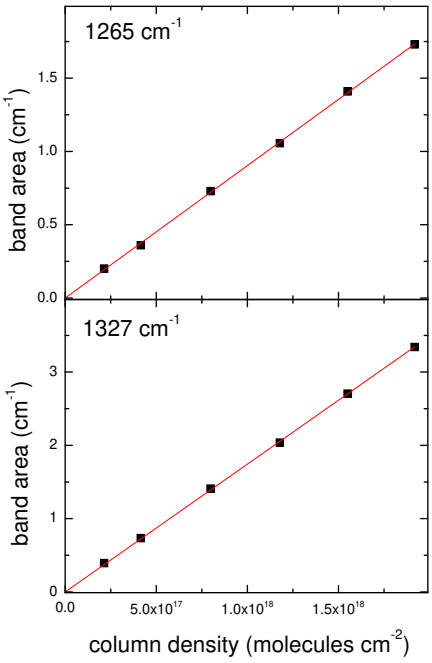

Figure 9: Measures of the P polarization band areas (1265 and 1327 cm^{-1}) versus the column density for the CH_2DOH deposited ice.

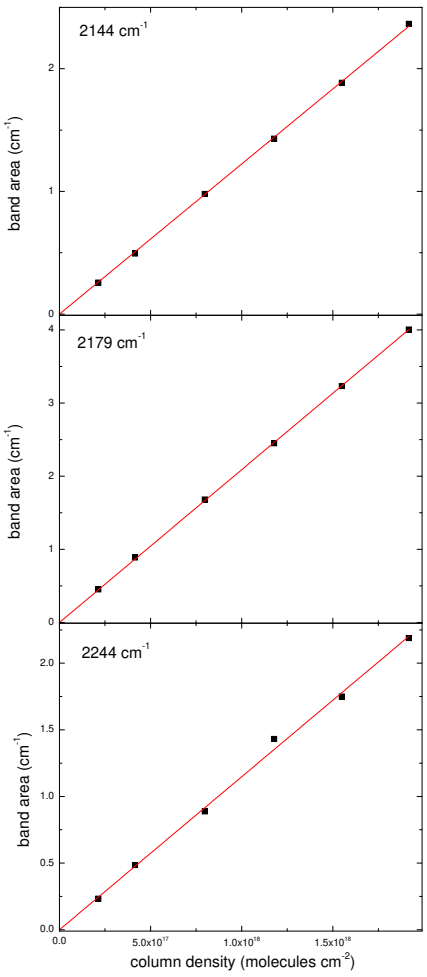

Figure 10: Measures of the P polarization band areas (2144, 2179 and 2244 cm^{-1}) versus the column density for the CH_2DOH ice.

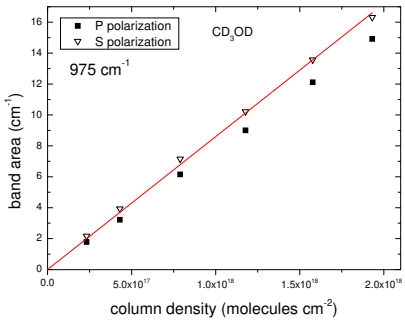

Figure 11: Measures of the CO stretching P and S polarization band areas versus the column density for the CD_3OD ice. The linear best fit is performed only on the S polarization data.

3.3. CH_2DOH:CO=1:4, CH_2DOH:H_2O=1:5 and CH_2DOH:CH_3OH=1:2 mixtures

In order to prepare the mixtures, the gas (CO) or vapors (H_2O, CH_2DOH and CH_3OH) were sequentially admitted in the mixing chamber. We used a vacuum piezo detector to determine the partial pressure of gas and vapors and hence the mixing ratio of the binary mixtures in the gas phase. In Fig. 12 the bands at 2144, 2179 and 2244 cm^{-1} are clearly distinguishable in all the spectra except for the CH_2DOH:CO=1:4 mixture, in which only the 2179 and 2244 cm^{-1} features are visible since the 2144 cm^{-1} band is masked by the very intense 2140 cm^{-1} CO band (e.g. Urso et al., 2016).

3.4. Temperature effects

All the mixtures were deposited at 17 K on a KBr substrate and they were warmed up at several intermediate temperature steps until their complete sublimation. The CH_2DOH was deposited at 17 K on KBr substrate and then it was warmed up at 40, 60, 80, 100, 110, 120, 130, 140 and 150 K. For each temperature step, spectra were acquired in P and S polarization. In Fig. 13(a), the CH_2DOH spectra acquired at 17 and 120 K are reported; a zoom on the CD stretching region is also reported in Fig. 13(b). From Fig. 13(a) it is evident that the bands width decreases and the bands intensity increases when the temperature increases. Furthermore, a splitting in the OH stretching region is observed at 120 K. From Fig. 13(b) it is also evident that the intensity of the bands at 2144 and 2179 cm^{-1} increases as the temperature is rised, whereas the intensity of the band at 2244 cm^{-1}

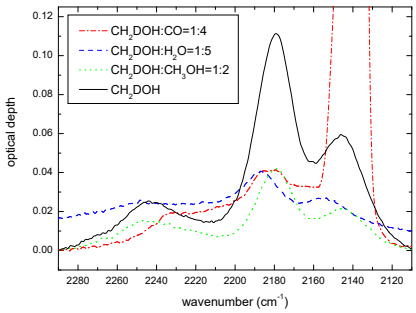

Figure 12: Profiles of the bands at 2144, 2179 and 2244 cm^{-1} for the spectra CH_2DOH:CO, CH_2DOH:H_2O, CH_2DOH:CH_3OH and CH_2DOH all taken in P polarization at 17 K. The spectra refer to samples of about the same thickness (~ 1 μm) except for the CH_2DOH:H_2O mixture which is ~ 0.6 μm thick.

decreases (see Suzuki and Inaba, 2017). These modifications are ascribed to the amorphous to crystalline transition which occurs at about 110 K. In our experimental conditions pure CH_2DOH sublimates at about 150 K.

In Fig. 14, a comparison between the spectra of CH_2DOH:CO, CH_2DOH:H_2O and CH_2DOH:CH_3OH at 17 and 120 K is reported.

4. Final remarks

Presently the knowledge on the chemical and physical properties of ice grain mantles in star forming regions as well as of the surface of airless bodies in the Solar System is mainly based on the comparison between astronomical and laboratory spectra. In particular, the main vibrational modes of H-, C-, N-, and O- bearing species can be identified in the mid-infrared range, and when band strength values are known it is possible to estimate the column density of a given species (Tielens and Allamandola, 1987). Here we have presented a novel experimental study on solid CH_2DOH pure and in astrophysical relevant mixtures. In particular we have measured the band strength values of its main features and studied the profile of the C-D stretching mode bands in astrophysical relevant mixtures. Even if solid CH_2DOH has not yet been detected in space, it is largely believed that it is present in solid form in star forming regions and it is expected to be detected by new generation IR telescopes. Our experimental results will contribute to its identification and to obtain an estimation of its column density.

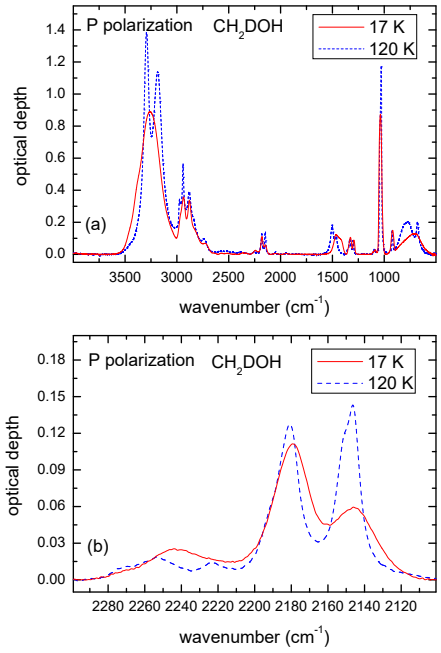

Figure 13: (a) CH_2DOH spectra at 17 K and 120 K. (b) Detail of the CD stretching modes vibration region (2300-2100 cm^{-1}). **The sample is about 1 μm thick.**

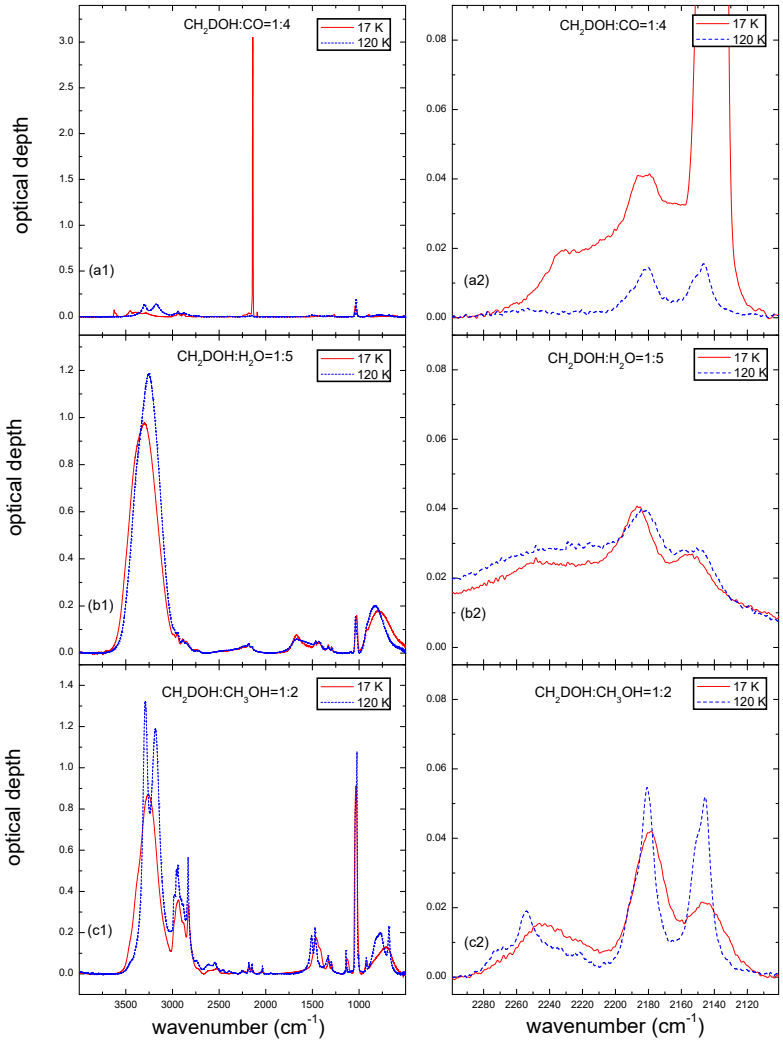

Figure 14: Comparison between spectra at 17 K and 120 K for the mixtures: (a1) CH_2DOH:CO, (b1) CH_2DOH:H_2O, and (c1) CH_2DOH:CH_3OH, (a2), (b2), and (c2) detail of the CD stretching modes vibration region (2300-2100 cm^{-1}) for the respective mixtures. **The samples are about 1 μm thick except than the CH_2DOH:H_2O mixture which is about 0.6 μm thick.**

5. Acknowledgements

This work has been supported by the project PRIN-INAF 2016 The Cradle of Life - GENESIS-SKA (General Conditions in Early Planetary Systems for the rise of life with SKA) and by the Italian Ministero dellIstruzione, dellUniversità e della Ricerca through the grant Progetti Premiali 2012-iALMA (CUP C52I13000140001).

R.G.U. acknowledges the CNES postdoctoral program and the ANR support from the grant RAHIIA SSOM (ANR-16-CE29-0015).

D.F. acknowledges the Brazilian foundation CNPq (Chamada Universal 2016 - Processo: 426929/2016-0) and FAPERJ (Programa Jovem Cientista do Nosso Estado 2017 - Processo: E-26/203.204/2017) for financial support.

References

Y. Aikawa, D. Kamuro, I. Sakon, Y. Itoh, H. Terada, J.A. Noble, K.M. Pontoppidan, H.J. Fraser, M. Tamura, R. Kandori, A. Kawamura, M. Ueno, AKARI observations of ice absorption bands towards edge-on young stellar objects, Astron. Astrophys. 538 id.A57 (2012) 12, DOI: 10.1051/0004-6361/201015999.

L.J. Allamandola, S.A. Sandford, A.G.G.M Tielens, T.M. Herbst, Infrared spectroscopy of dense clouds in the C-H stretch region - Methanol and "Diamonds", Astrophys. J. 399 (1992) 134-146, DOI: 10.1086/171909.

K. Altwegg, H. Balsiger, A. Bar-Nun et al., 67P/Churyumov-Gerasimenko, a Jupiter family comet with a high D/H ratio, Science 347 (2015) 1261952, DOI: 10.1126/science.1261952.

K. Altwegg, H. Balsiger, A. Bar-Nun et al., D_2O and HDS in the coma of 67P/Churyumov-Gerasimenko, Phil. Trans. R. Soc. 375 (2017) 20160253, DOI: 10.1098/rsta.2016.0253.

G.A. Baratta, M.E. Palumbo, Infrared optical constants of CO and CO_2 thin icy films, JOSA A 15 (1998) 307, DOI: 10.1364/JOSAA.15.003076.

G.A. Baratta, M.E. Palumbo, The profile of the bending mode band in solid CO_2, Astron. Astrophys. 608 (2017) A81, DOI: 10.1051/0004-6361/201730945.

C.J. Bennett, S.H. Chen, B.J. Sun, A.H.H. Chang, and R.I. Kaiser, Mechanistical Studies on the Irradiation of Methanol in Extraterrestrial Ices, Astrophys. J. 660 (2007) 1588-1608, DOI: 10.1086/511296.

E. Bianchi, C. Codella, C. Ceccarelli, V. Taquet, S. Cabrit, F. Bacciotti, R. Bachiller, E. Chapillon, F. Gueth, A. Gusdorf, B. Lefloch, S. Leurini, L. Podio, K.L.J. Rygl, B. Tabone, M. Tafalla, Deuterated methanol on a solar system scale around the HH212 protostar, Astron. Astrophys. 606 (2017) L7, DOI: 10.1051/0004-6361/201731404.

A.C.A. Boogert, P. Ehrenfreund, P.A. Gerakines, A.G.G.M. Tielens, D.C.B. Whittet, W.A. Schutte, E.F. van Dishoeck, Th. de Graauw, L. Decin, T. Prusti, ISOSWS observations of interstellar solid $^{13}CO_2$: heated ice and the Galactic $^{12}C/^{13}C$ abundance ratio, Astron. Astrophys. 353 (2000) 349-362.

A.C.A. Boogert, G.A. Blake, A.G.G.M. Tielens, High-resolution 4.7 micron Keck/NIRSPEC spectra of protostars. II. Detection of the ^{13}CO isotope in icy grain mantles, Astrophys. J. 577 (2002) 271, DOI: 10.1086/342176.

A.C.A. Boogert, P.A. Gerakines, D.C.B. Whittet, Observations of the icy universe, Ann. Rev. Astron. Astrophys. 53 (2015) 541-581, DOI: 10.1146/annurev-astro-082214-122348.

P. Caselli, C. Ceccarelli, Our astrochemical heritage, Astron. Astrophys. Review 20 (2012) 56, DOI: 10.1007/s00159-012-0056-x.

C. Ceccarelli, Millimeter and infrared observations of deuterated molecules, Planetary and Space Science 50 (2002) 1267 1273, DOI: 10.1016/S0032-0633(02)00093-4.

C. Ceccarelli, P. Caselli, D. Bockelée-Morvan, O. Mousis, S. Pizzarello, F. Robert, D. Semenov, Deuterium Fractionation: the Ariadnes Thread from the Pre-collapse Phase to Meteorites and Comets today, Protostars and Planets 914 (2014) 859, DOI: 10.2458/azu_uapress_9780816531240-ch037.

E. Dartois, W.F. Thi,T.R. Geballe, D. Deboffle, L. d'Hendecourt, E. van Dishoeck, Revisiting the solid HDO/H_2O abundances, Astron. Astrophys. 399 (2003) 1009-1020, DOI: 10.1051/0004-6361:20021558.

M.N. Drozdovskaya, E.F. van Dishoeck, J.K. Jrgensen, U. Calmonte, M.H.D. van der Wiel, A. Coutens, H. Calcutt, H.S.P. Müller, P. Bjerkeli, M.P.

Persson, S.F. Wampfler, K. Altwegg, The ALMA-PILS survey: the sulphur connection between protostars and comets: IRAS 16293-2422 B and 67P/Churyumov-Gerasimenko, Monthly Notices of the Royal Astronomical Society 476 (2018) 4 4949, DOI: 10.1093/mnras/sty462.

M. Falk, E. Whalley, Infrared Spectra of Methanol and Deuterated Methanols in Gas, Liquid, and Solid Phases, The Journal of Chemical Physics 34 (1961) 1554, DOI: 10.1063/1.1701044.

F. Fontani, C. Codella, C. Ceccarelli, B. Lefloch, S. Viti, M. Benedettini, The L1157-B1 astrochemical laboratory: Measuring the true formaldehyde deuteration on grain mantles, Astrophys. J. Letters 788 (2014) L43, DOI: 10.1088/2041-8205/788/2/L43.

F. Fontani, G. Busquet, A. Palau, P. Caselli, A. Sanchez-Monge, J.C. Tan, M. Audard, Deuteration and evolution in the massive star formation process. The role of surface chemistry, Astron. Astrophys. 575 (2015) A87, DOI: 10.1051/0004-6361/201424753.

D. Fulvio, B. Sivaraman, G.A. Baratta, N.J. Mason, Novel measurements of refractive index, density and mid-infrared band strength values for solid O_2, N_2O and NO_2:N_2O_4 mixtures, Spectrochim. Acta A 72 1007, DOI: 10.1016/j.saa.2008.12.030.

E. Furi, B. Marty, Nitrogen isotope variations in the Solar System, Nat. Geosci. 8 (2015) 515, DOI: 10.1038/ngeo2451.

P.A. Gerakines, W.A. Schutte, J.M. Greenberg, E. F. van Dishoeck, The infrared band strengths of H_2O, CO and CO_2 in laboratory simulations of astrophysical ice mixtures, Astron. Astrophys. 296 (1995) 810-818.

E.L. Gibb, D. C. B. Whittet, A.C.A. Boogert, A.G.G.M. Tielens, Interstellar ice: The Infrared Space Observatory legacy, Astrophys. J. Suppl. Series, 151 (2004) 35-73, DOI: 10.1086/381182.

F.C. Gillett, W.J. Forrest, Spectra of the Becklin-Neugebauer point source and the Kleinmann-Low nebula from 2.8 to 13.5 microns, Astrophys. J. 179 (1973) 483 - 491.

J.M. Greenberg, What are comets made of - A model based on interstellar dust, Comets. 83-13376 03-90 (1982) 131-163.

P. Hartogh Hartogh, D.C. Lis, D. Bockelée-Morvan, M. de Val-Borro, N. Biver, M. Kppers, M. Emprechtinger, E.A. Bergin, J. Crovisier, M. Rengel, R. Moreno, S. Szutowicz, G.A. Blake, Ocean-like water in the Jupiter-family comet 103P/Hartley 2, Nature 478 (2011) 218-220, DOI: 10.1038/nature10519.

D.M. Hudgins, S.A. Sandford, L.J. Allamandola, and A. G. G. M. Tielens, Mid- and far-infrared spectroscopy of ices: Optical constants and integrated absorbances, Astrophys. J. Suppl. Series, 86 (1993) 713-870.

O. Kerkhof, W.A. Schutte, P. Ehrenfreund, The infrared band strengths of CH_3OH, NH_3 and CH_4 in laboratory simulations of astrophysical ice mixtures, Astron. Astrophys. 346 (1999) 990-994.

M.J. Loeffler, M.H. Moore, P.A. Gerakines, The Effects of Experimental Conditions on the Refractive Index and Density of Low-temperature Ices: Solid Carbon Dioxide, Astrophys. J. 827 (2016) 98, DOI: 10.3847/0004-637X/827/2/98.

R. Luna, G. Molpeceres, J. Ortigoso, M.A. Satorre, M. Domingo, B. Maté, Densities, infrared band strengths, and optical constants of solid methanol, Astron. Astrophys. 617 (2018) A116, DOI: 10.1051/0004-6361/201833463.

K.M. Merrill, B.T. Soifer, Spectrophotometric Observations of a highly absorbed object in Cygnus, Astrophys. J. Letters 189 (1974) L27-L30.

P. Modica, & M.E. Palumbo, Formation of methyl formate after cosmic ion irradiation of icy grain mantles, Astron. Astrophys. 519 (2010) A22, DOI: 10.1051/0004-6361/201014101.

G. Mulas, G.A. Baratta, M.E. Palumbo, G. Strazzulla, Profile of CH_4 IR bands in ice mixtures, Astron. Astrophys. 333 (1998) 1025-1033.

K.I. berg, H.J. Fraser, A.C.A. Boogert, S. E. Bisschop, G.W. Fuchs, E.F. van Dishoeck, H. Linnartz, Effects of CO_2 on H_2O band profiles and band strengths in mixed H_2O:CO_2 ices, Astron. Astrophys. 462 (2007) 1187-1198, DOI: 10.1051/0004-6361:20065881.

K.I. berg, V.V. Guzmn, K. Furuya, C. Qi, Y. Aikawa, S.M. Andrews, R. Loomis, D.J. Wilner, The comet-like composition of a protoplanetary disk

as revealed by complex cyanides, Nature 520 (2015) 198, DOI: 10.1038/nature14276.

M.E. Palumbo, A.C. Castorina, G. Strazzulla, Ion irradiation effects on frozen methanol (CH_3OH), Astron. Astrophys. 342 (1999) 551562.

M.E. Palumbo, G.A. Baratta, M.P. Collings, M.R.S. McCoustra, The profile of the 2140 cm^{-1} solid CO band on different substrates, Physical Chemistry Chemical Physics, Vol. 8 (2006) 279-284.

B. Parise, T. Simon, E. Caux, E. Dartois, C. Ceccarelli, J. Rayner, A.G.G.M. Tielens, Search for solid HDO in low-mass protostars, Astron. Astrophys. 410 (2003) 897-904, DOI: 10.1051/0004-6361:20031277.

W.A. Schutte, L.J. Allamandola, S.A. Sandford, An experimental study of the organic molecules produced in cometary and interstellar ice analogs by thermal formaldehyde reactions, Icarus 104 (1993) 118-137.

A. Serrallach, R. Meyer, Hs.H. Gunthard, Methanol and Deuterated Species: Infrared Data, Valence Force Field, Rotamers, and Conformation, Journal of molecular spectroscopy 52 (1974) 94-129.

T. Shimoaka, Y. Katsumoto, Blue Shift of the Isolated CD Stretching Band of CH_2DOH in Water Induced by Changes in the Hydrogen-Bonding Pattern, J. Phys. Chem. A 114 (2010) 1197111976, DOI: 10.1021/jp1065133.

H. Suzuki, A. Inaba, Isotopic localization of the partially deuterated methyl group in solid methanol and methyl iodide, The Journal of Chemical Physics 146 (2017) 174501, DOI: 10.1063/1.4982210.

T.C. Teixeira, J.P. Devlin, V. Buch, J.P. Emerson, Discovery of solid HDO in grain mantles, Astron. Astrophys. 347 (1999) L19-L22.

A.G.G.M. Tielens, L.J. Allamandola, Evolution of interstellar dust, in: G.E. Morfill, M. Scholer (Eds.), Physical Processes in Interstellar Clouds, D. Reidel Publishing Company, Dordrecht, 1987, pp. 333-376.

A.G.G.M. Tielens, A.T. Tokunaga, T.R. Geballe, F. Baas, Interstellar solid CO - Polar and nonpolar interstellar ices, Astrophys. J. 381 (1991) 181-199.

R.G. Urso, C. Scirè, G.A. Baratta, G. Compagnini, M.E. Palumbo, Combined infrared and Raman study of solid CO, Astron. Astrophys. 594 (2016) A80, DOI: 10.1051/0004-6361/201629030.

R.G. Urso, M.E. Palumbo, G.A. Baratta, C. Scirè, G. Strazzulla, Solid deuterated water in space: detection constraints from laboratory experiments, Monthly Notices of the Royal Astronomical Society 479 (2018) 130140, DOI: 10.1093/mnras/sty1428.

B.E. Wood, J.A. Roux, Infrared optical properties of thin H_2O, NH_3, and CO_2 and cryofilms, JOSA 72 (1982) 720-728, DOI: 10.1364/JOSA.72.000720.